Microsomal Glutathione Transferase 1 Protects Against Toxicity Induced by Silica Nanoparticles but Not by Zinc Oxide Nanoparticles

Jingwen Shi,[†] Hanna L. Karlsson,[†] Katarina Johansson,[†] Vladimir Gogvadze,[†] Lisong Xiao,[‡] Jiangtian Li,[‡] Terrance Burks,[§] Alfonso Garcia-Bennett,[⊥] Abdusalam Uheida,[§] Mamoun Muhammed,[§] Sanjay Mathur,[‡] Ralf Morgenstern,[†] Valerian E. Kagan,[∥] and Bengt Fadeel[†,*]

[†]Institute of Environmental Medicine, Karolinska Institutet, 17177 Stockholm, Sweden, [‡]Inorganic and Materials Chemistry, University of Cologne, 50939 Cologne, Germany, [§]Functional Materials Microelectronics and Applied Physics, School of Information and Communication Technology, Royal Institute of Technology, 16440 Kista, Sweden, [⊥]Nanotechnology and Functional Materials, Ångström Laboratory, Uppsala University, 75121 Uppsala, Sweden, and [∥]Department of Environmental and Occupational Health, University of Pittsburgh, Pittsburgh, Pennsylvania 15219, United States

ABSTRACT Microsomal glutathione transferase 1 (MGST1) is an antioxidant enzyme located predominantly in the mitochondrial outer membrane and endoplasmic reticulum and has been shown to protect cells from lipid peroxidation induced by a variety of cytostatic drugs and pro-oxidant stimuli. We hypothesized that MGST1 may also protect against nanomaterial-induced cytotoxicity through a specific effect on lipid peroxidation. We evaluated the induction of cytotoxicity and oxidative stress by TiO_2, CeO_2, SiO_2, and ZnO in the human MCF-7 cell line with or without overexpression of MGST1. SiO_2 and ZnO nanoparticles caused dose- and time-dependent toxicity, whereas no obvious cytotoxic effects were induced by nanoparticles of TiO_2 and CeO_2. We also noted pronounced cytotoxicity for three out of four additional SiO_2 nanoparticles tested. Overexpression of MGST1 reversed the cytotoxicity of the main SiO_2 nanoparticles tested and for one of the supplementary SiO_2 nanoparticles but did not protect cells against ZnO-induced cytotoxic effects. The data point toward a role of lipid peroxidation in SiO_2 nanoparticle-induced cell death. For ZnO nanoparticles, rapid dissolution was observed, and the subsequent interaction of Zn^{2+} with cellular targets is likely to contribute to the cytotoxic effects. A direct inhibition of MGST1 by Zn^{2+} could provide a possible explanation for the lack of protection against ZnO nanoparticles in this model. Our data also showed that SiO_2 nanoparticle-induced cytotoxicity is mitigated in the presence of serum, potentially through masking of reactive surface groups by serum proteins, whereas ZnO nanoparticles were cytotoxic both in the presence and in the absence of serum.

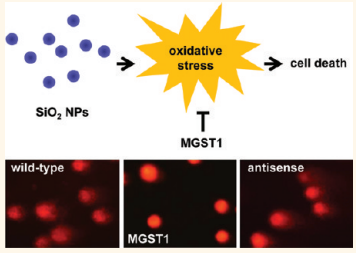

KEYWORDS: engineered nanoparticles · oxidative stress · lipid peroxidation · microsomal glutathione transferase 1

Engineered nanomaterials are commonly defined as materials in the size range of 1−100 nm in one or more dimensions. However, a recent study argued that novel size-dependent properties alone, rather than particle size, should be the primary criterion in any definition of nanoparticles, and the authors suggested that there is a critical size, typically 30 nm or less, at which these new properties appear, at least for inorganic nanoparticles.[1] Nanoparticles may trigger cytotoxic effects, and oxidative stress induction has been proposed as a common paradigm for the cellular toxicity of nanoparticles.[2,3] Indeed, evidence has been provided that oxidative stress is associated with nanoparticle-induced toxicity *in vitro* and *in vivo*.[4,5] However, it is unclear whether oxidative stress associated with nanomaterials is the direct cause of cytotoxicity or a secondary effect of cellular insult.[6] This distinction is important because it has implications for whether antioxidant countermeasures against nanoparticle toxicity are likely to succeed or not.

Microsomal glutathione transferase 1 (MGST1) is a detoxification enzyme that belongs to the MAPEG (membrane-associated proteins in eicosanoid and glutathione metabolism) superfamily, and it is highly expressed in liver.[7] In rat liver, MGST1 constitutes 3% of the endoplasmic reticulum (ER) membrane proteins and 5% of the proteins of the outer membrane of mitochondria.[8] The enzyme displays both glutathione transferase and glutathione peroxidase activity and is suggested to protect against cellular damage induced by a range of stimuli, including cytostatic drugs.[9] Previously, it has been shown that MGST1 protects against oxidative stress induced by various pro-oxidant stimuli in a variety of cellular models.[10,11] Specifically, MGST1 has been proposed to play an important role in protection of membranes against lipid peroxidation.[12,13] Indeed, we recently reported that MGST1 overexpressing cells

* Address correspondence to bengt.fadeel@ki.se.

Received for review November 8, 2010 and accepted February 4, 2012.

Published online February 05, 2012
10.1021/nn2021056

are significantly protected against agents that are known to induce lipid peroxidation (*e.g.*, cumene hydroperoxide and *tert*-butylhydroperoxide).[14] Here, we hypothesize that MGST1, a highly abundant protein, can also protect against nanoparticle-induced oxidative stress, through the protection against lipid peroxidation in cell membranes. To this end, we selected a panel of common, commercially available nanoparticles of different chemical composition, TiO_2, CeO_2, ZnO, and SiO_2, and applied these in a previously established cellular model with overexpression of MGST1.[9] Importantly, the overexpression of MGST1 in this model is at a physiologically relevant level, 10 times lower than in rat liver, and comparable to the expression of this enzyme in many extrahepatic organs.[9,10] MGST1 overexpression was found to protect cells against SiO_2-induced oxidative stress and cell death but not against ZnO nanoparticle-induced cell death. We observed rapid dissolution of ZnO nanoparticles in cell culture medium, and the cytotoxic effects could thus be related to the presence of intracellular Zn^{2+} ions, as suggested by other investigators.[4] We then tested the hypothesis that the protective effect is a general one for amorphous SiO_2 nanoparticles. However, overexpression of MGST1 did not protect against all particles tested. The reason for these differences was investigated with respect to particle characteristics such as the degree of dissolution, zeta-potential, and agglomeration state. Taken together, these studies improve our understanding of the role of oxidative stress in nanomaterial-induced toxicity and point toward potential antioxidant strategies to overcome such adverse effects. This work also underscores the importance of a case-by-case assessment of nanomaterial toxicity coupled with thorough material characterization.

RESULTS

Physicochemical Characterization of Metal Oxide Nanoparticles. The TEM analysis of TiO_2, CeO_2, ZnO, and SiO_2 nanoparticles confirmed particle shapes and primary particle sizes (Figure 1). The hydrodynamic size of the particles in cell culture medium with or without serum was also determined. All nanoparticles tested appeared to aggregate in the absence of serum, although to a lesser extent in the case of SiO_2 nanoparticles. However, when serum was added to the medium, the particle size was stabilized (Table 1). Surface charge and the degree of endotoxin contamination were also determined for each nanoparticle (Table 1). In addition to this primary set of particles, we included additional SiO_2 nanoparticles, as noted below, and the characteristics of these particles are reported in Supporting Information.

Cytotoxicity of Metal Oxide Nanoparticles. Cytotoxicity of TiO_2, CeO_2, ZnO, and SiO_2 nanoparticles toward the MCF-7 cell line was evaluated using the 3-[4,5-dimethylthiazol-2yl]-2,5-diphenyltetrazolium bromide (MTT) assay for cells cultured in the presence (Figure 2A) or absence (Figure 2B) of serum. TiO_2 and CeO_2 nanoparticles displayed little toxicity at doses up to 200 μg/mL, irrespective of whether serum was present. ZnO nanoparticles induced a sharp decrease in cell viability in the absence of serum, with an IC_{50} of 40 μg/mL. Upon supplementation of the cell culture medium with 10% fetal bovine serum, the IC_{50} was 100 μg/mL (Figure 2A,B). Dose-dependent toxicity was also induced by the SiO_2 nanoparticles when MCF-7 cells were cultivated in the absence of serum, whereas the presence of serum in the medium completely masked this toxicity (Figure 2A,B). The range of doses in the present study (up to 200 μg/mL) is in the range of doses commonly applied for *in vitro* testing of engineered nanoparticles.[15] When higher doses were tested (up to 500 μg/mL), we noted that CeO_2 nanoparticles also impaired cell viability, whereas TiO_2 nanoparticles remained noncytotoxic (data not shown).

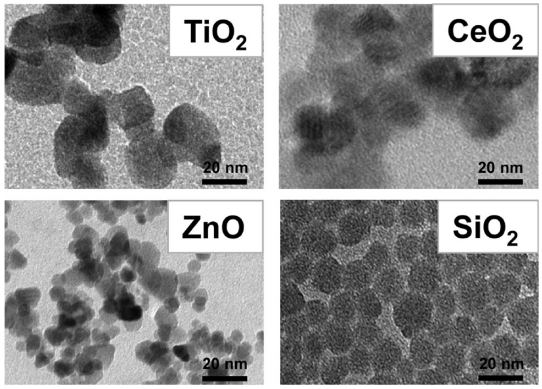

Figure 1. TEM images of the metal oxide nanoparticles TiO_2, CeO_2, ZnO, and SiO_2. Scale bar: 20 nm.

TEM images showed clear evidence of cellular uptake of the TiO_2 and CeO_2 nanoparticles after 2 h, and particles were mainly observed within membrane-bound vesicles (endosomes) (Figure 3). However, no particles could be observed in cells following exposure to ZnO nanoparticles, likely due to their rapid intracellular dissolution. SiO_2 nanoparticles were clearly observed at the cell surface, but their uptake was difficult to determine due to the presence of similar electron-dense structures (ribosomes) in control cells (Figure 3, Supporting Information Figure 1A). To gain a better understanding of cellular uptake of the SiO_2 nanoparticles, the particles were labeled with FITC as described in Materials and Methods and uptake was monitored using flow cytometry. Trypan blue was utilized to quench extracellular fluorescence. The results revealed cellular uptake of the SiO_2–FITC particles, and uptake was higher in the absence of serum (Supporting Information Figure 1B). Cellular uptake was confirmed by fluorescence microscopy (Supporting Information Figure 1C). These results show that the lack of toxicity for the TiO_2 and CeO_2 nanoparticles was not due to a

TABLE 1. Physicochemical Characterization of Metal Oxide Nanoparticles

chemical formula	crystallinity	size distribution[a]	hydrodynamic size[b]	charge (pH 7.4)[c]	endotoxin[d]	dissolution[e] (%) −serum	dissolution[e] (%) +serum
TiO_2	rutile/anatase	29.2 ± 10 nm	(+) 1.38 ± 0.03 μm (−) 2.3 ± 0.2 μm	−14.6	no	0.02	0.35
CeO_2	crystalline	23.4 ± 4 nm	(+) 40 ± 3 nm (−) 1.4 ± 0.02 μm	27.6	no	0	1.2
ZnO	hexagonal	15.5 ± 4 nm	(+) 28 ± 4 nm (−) 1.1 ± 0.2 μm	19.7	no	12.3	17.7
SiO_2	amorphous	12.0 ± 2 nm	(+) 30 ± nm (−) 70.4 ± 0.2 nm	−34.9	1 ng/mL	6.9	6.4

[a] Size distribution determined by TEM. [b] Hydrodynamic size as measured by DLS, in the presence (+) or absence (−) of 10% fetal bovine serum (FBS). [c] Charge measured by zeta-potential. [d] Endotoxin contamination was evaluated by LAL test, as described in Materials and Methods. [e] Representative data from 2−3 independent experiments are shown. Dissolution of the particles was evaluated at 37 °C in the presence or absence of 10% FBS, as indicated. For ZnO nanoparticles, dissolution was also evaluated in H_2O (25 °C), PBS (25 °C), and cell culture medium (25 °C), and the following values were recorded (%): 25.9 (H_2O); 0.0 (PBS); 12.1 (CCM 25 °C) (data representative of 2 independent experiments).

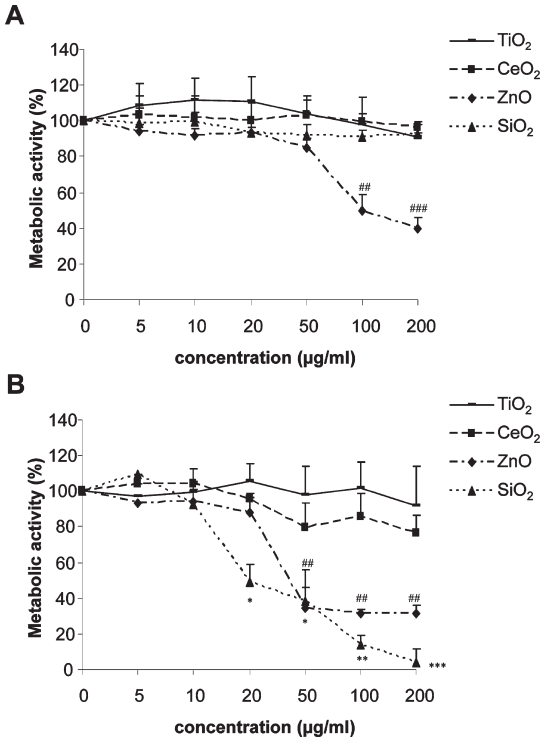

Figure 2. Cytotoxicity induced by metal oxide nanoparticles in MCF-7 cells. Dose-dependent cytotoxicity induced by TiO_2, CeO_2, ZnO, and SiO_2, in the presence (A) or absence (B) of serum at 24 h, assessed as metabolic activity by MTT assay. The results are expressed by mean values ± SD (*n* = 3−4); *<0.05, **<0.01, *<0.001 (for SiO_2 compared to control, *i.e.*, no treatment); ##<0.01, ###<0.001 (for ZnO compared control).**

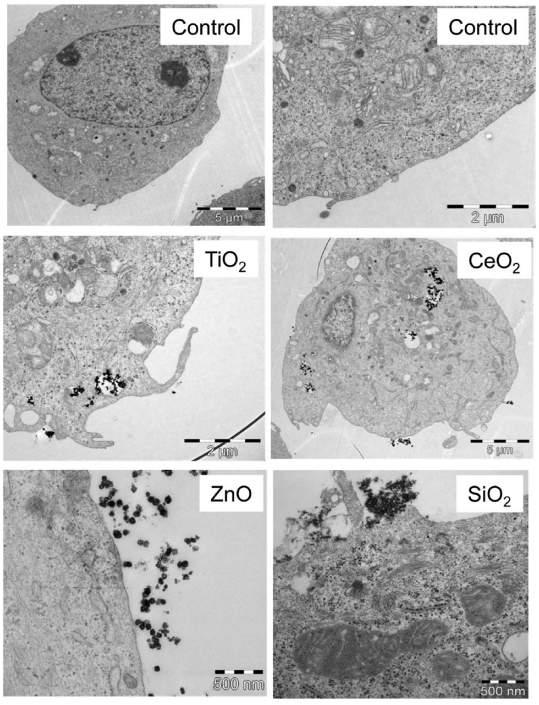

Figure 3. Particle uptake following exposure of MCF-7 cells. Uptake of TiO_2 and CeO_2 nanoparticles was evident, while no evidence of cellular uptake of intact ZnO nanoparticles was observed, likely due to rapid dissolution. SiO_2 nanoparticles appeared to interact with the plasma membrane, but uptake was difficult to ascertain due to the similarity of the particles to other cellular structures in terms of size, shape, and electron density. Cells were incubated with particles (50 μg/mL) for 2 h. Scale bars for control cells are 5 and 2 μm (left and right, respectively), 2 μm for TiO_2, 5 μm for CeO_2, and 500 nm for ZnO as well as SiO_2.

lack of cellular uptake. The increase in uptake of SiO_2 nanoparticles in serum-deprived cultures could provide a partial explanation for the increased toxicity under these conditions (Figure 2A,B), but these results do not explain why serum completely blocks cytotoxicity, and it is therefore likely that other factors also contribute.

MGST1 Protects Against SiO_2 Nanoparticle-Induced Cytotoxicity. To assess the role of the antioxidant enzyme MGST1, the human MCF-7 cell line was stably transfected with rat liver MGST1 (sense cell line) or with antisense against rat-MGST1 (antisense cell line).[9] The overexpression of MGST1 was confirmed by Western blotting using a polyclonal rabbit anti-rat MGST1 (Figure 4A). Cumene hydroperoxide (CuOOH) is a known substrate of MGST1, and the glutathione peroxidase activity of MGST1 protects against the cytotoxic effects of CuOOH.[10] This was

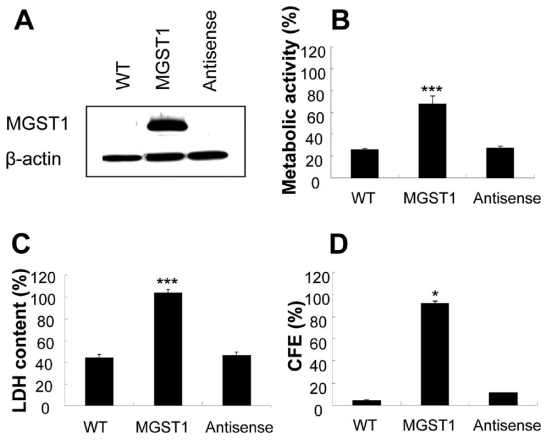

Figure 4. MGST1 protects against cytotoxicity induced by CuOOH. (A) Western blot confirmation of MGST1 overexpression (17 kDa) using a specific antirat MGST1 antibody. β-Actin (42 kDa) was used as loading control. Cytotoxicity induced by CuOOH, measured as (B) metabolic activity using the MTT assay (50 μM CuOOH, 1 h incubation), (C) LDH release (50 μM CuOOH, 1 h incubation), and (D) colony formation (CFE) assay (5 μM CuOOH, 3 h incubation and further incubation for 7 days), is prevented by MGST1.

confirmed in the present study using the standard MTT assay, the lactate dehydrogenase (LDH) release assay, and the colony formation efficiency (CFE) assay, and CuOOH was therefore used as a positive control in all subsequent experiments (Figure 4B–D). MGST1 overexpression afforded significant protection against SiO_2 nanoparticle-induced cytotoxicity when the cells were cultured in the absence of serum for 24 h, as evidenced by the MTT assay (Figure 5A). Moreover, since certain nanoparticles have been suggested to interfere with the MTT assay,[16] and because reduction of MTT by glutathione transferase also has been reported,[17] cytotoxicity was also evaluated using the LDH assay, and this assay revealed the same protective effect of MGST1 (Figure 5C). Furthermore, to confirm whether this can also occur in more physiological conditions with serum present, the CFE assay was utilized. Of note, when the CFE assay is applied, cells are exposed for 24 h to nanoparticles, followed by wash-out of the particles and replenishment of cell culture medium, and the number of cell colonies is counted after 7 days, as an indicator of cell survival/cell proliferation. As seen in Figure 5E, MGST1 overexpression also prevented the long-term cytotoxicity of SiO_2 nanoparticles. We obtained similar results when applying the fluorescent dye, propidium iodide (PI), to monitor membrane permeability following exposure to SiO_2 nanoparticles (data not shown). However, MGST1 overexpression was not able to reduce ZnO nanoparticle-induced cytotoxicity, as determined using the short-term cell viability assays (MTT, LDH) and the long-term assay (CFE) (Figure 5B,D,F). In addition, overexpression of MGST1 did not protect against the cytotoxicity induced by high doses (500 μg/mL) of CeO_2 nanoparticles (data not shown).

We also tested the possibility that Zn^{2+} could directly inhibit MGST1 activity so that the enzyme is not protective. To this end, the activity of MGST1 was tested by an assay based on the GST-catalyzed reaction between GSH and the GST substrate, CDNB. The IC_{50} of MGST1 for Zn sulfate was determined to be 0.51 mM (0.42–0.64, 95% confidence interval). Sodium sulfate did not inhibit the enzyme at 5 mM, suggesting that Zn^{2+} caused the inhibition. However, the non-enzymatic reaction between the substrate CDNB and GSH was completely inhibited upon the addition of Zn^{2+}, suggesting that Zn^{2+} interferes with these substrates likely due to the fact that Zn^{2+} forms a strong complex with GSH.

MGST1 Reverses SiO_2 Nanoparticle-Induced Oxidative Stress. Mitochondria are the main cellular source of reactive oxygen species (ROS) production and also one of the major sites of MGST1 expression, along with the ER.[8] To further explore the cytotoxic effects of SiO_2 and ZnO nanoparticles, we investigated mitochondrial ROS production and respiration/oxygen consumption. MGST1 overexpression reversed SiO_2-induced ROS production, as determined by the MitoSOX assay (Figure 6A), and dissipation of the mitochondrial membrane potential, as evidenced by the TMRE assay (Figure 7A). Moreover, MGST1 overexpression resulted in a decrease of the SiO_2-triggered inhibition of mitochondrial oxygen consumption, although the differences did not reach statistical significance (Supporting Information Figure 3A,B). In contrast, MGST1 overexpression did not reverse ZnO nanoparticle-induced mitochondrial ROS production (Figure 6B) or the impairment of mitochondrial respiration triggered by ZnO (Supporting Information Figure 3C,D).

To further investigate the induction of oxidative stress, we utilized the C_{11}-BODIPY$^{581/591}$ assay as a surrogate marker of lipid peroxidation,[18] and the fpg-comet assay for oxidative DNA damage.[19] As shown in Figure 6C,D, overexpression of MGST1 protected against lipid peroxidation triggered by SiO_2 nanoparticles but not against ZnO nanoparticles. Moreover, SiO_2 nanoparticle-induced oxidative DNA damage was reversed by MGST1 (Figure 7B,C). The effect of ZnO nanoparticles on DNA damage could not be assessed using the fpg-comet assay; indeed, interactions between nanoparticles and the fpg-comet assay have been described.[20] Nevertheless, our results show that MGST1 overexpression protects MCF-7 cells from SiO_2 nanoparticle-induced lipid peroxidation, mitochondrial impairment, and oxidative DNA damage.

Next, we studied the effects of SiO_2 nanoparticles on glutathione (GSH) levels using the ThioGlo-1 assay for measurement of intracellular reduced GSH.[21] In healthy cells, more than 90% of the total glutathione pool is in the reduced form (GSH) and less than 10% exists in the disulfide form (GSSG). An increased GSSG-to-GSH ratio is considered indicative of oxidative stress.

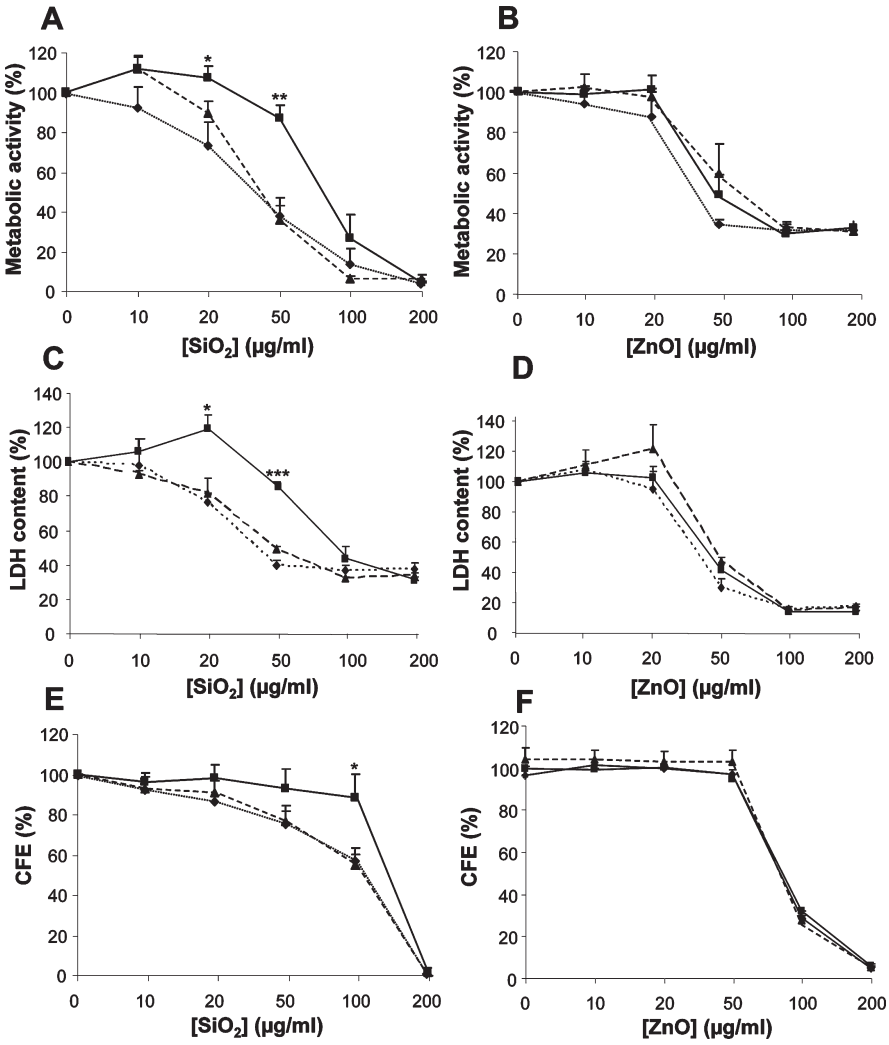

Figure 5. MGST1 protects against SiO_2 nanoparticle-induced cytotoxicity but not ZnO nanoparticle-induced cytotoxicity. MGST1 protection against nanoparticle-induced cytotoxicity at 24 h was assessed using MTT assay for assessment of metabolic activity (A,B), LDH assay to monitor cell membrane damage (C,D), and CFE assay to monitor the late effects of particle exposure (24 h exposure, followed by a further 7 day incubation) (E,F). MGST1 overexpressing cells are indicated by filled squares and solid line, antisense transfected cells by triangles and dashed line, and MCF-7 wild-type cells by diamonds and dotted line. The results are expressed as mean values ± SD (n = 3−4); *<0.05, **<0.01, *<0.01.**

As seen in Figure 8A, overexpression of MGST1 protected against the depletion of GSH induced by SiO_2 nanoparticles. The increased GSH level in MGST1 overexpressing cells following treatment with SiO_2 nanoparticles is most likely due to the fact that less GSH is consumed as less lipid peroxides are formed (Figure 8A). To exclude the possibility that the protective function of MGST1 is merely a result of resetting of the threshold of GSH in the cell upon overexpression of this enzyme, we manipulated the level of GSH by addition of buthionine-[S, R]-sulfoximine (BSO), a GSH-depleting agent (Figure 8B). This treatment, however, did not affect the sensitivity of the cells to SiO_2 nanoparticle-induced cytotoxicity (Figure 8C). Moreover, supplementation of the cell culture medium with *N*-acetylcysteine (NAC), a precursor of GSH, did not protect cells against SiO_2 nanoparticle-induced cell death, as determined by the MTT assay (Figure 8D). Hence, we conclude that overexpression of MGST1 protects specifically against SiO_2 nanoparticle-induced cytotoxicity but not against ZnO nanoparticle-induced cytotoxicity in this cell model.

ZnO Nanoparticles Undergo Rapid Dissolution in Cell Culture. To assess whether any differences in physicochemical characteristics between SiO_2 nanoparticles and ZnO nanoparticles may account for the observed differences in protection against cytotoxicity by MGST1 overexpression, we tested whether the nanoparticles have an inherent ability to generate ROS. This was achieved in a cell-free assay using the fluorescent probe, DCFH-DA, as described previously.[22] Hydrogen peroxide and Cu nanoparticles were both included as positive controls. The results show clearly that ZnO nanoparticles are capable of generating ROS in a dose-dependent manner, whereas the SiO_2 nanoparticles do not display the same reactivity (Supporting Information Figure 4A).

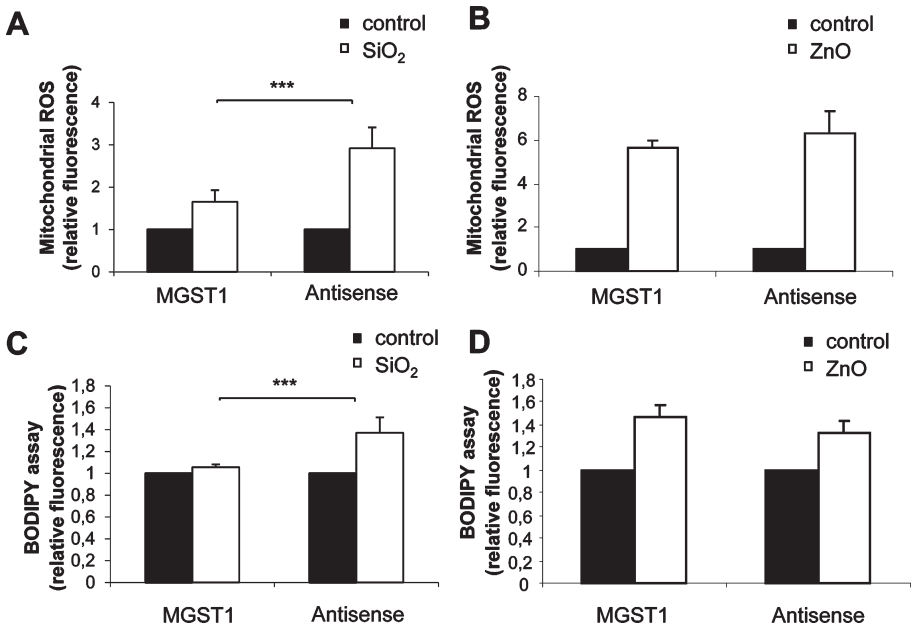

Figure 6. MGST1 protects against SiO_2 nanoparticle-induced but not ZnO nanoparticle-induced mitochondrial ROS production (A,B) and lipid peroxidation (C,D). Cells were incubated with 20 μg/mL nanoparticles for 2 h in the absence of serum. MitoSOX was used for measurement of mitochondria-specific superoxide generation and C_{11}-BODIPY$^{581/591}$ was used as a surrogate marker for lipid peroxidation; *<0.01.**

Xia *et al.* have provided evidence of rapid dissolution of ZnO nanoparticles in cell culture medium and in endosomes.[4] To further assess differences between the nanoparticles included in the present study, we measured Zn^{2+} leaching in H_2O (25 °C), PBS (25 °C), and cell culture medium (25 and 37 °C) by ICP (Table 1). These experiments showed that the dissolution of ZnO nanoparticles was highest when the particles were dispersed in H_2O. Moderate levels of Zn^{2+} leaching were observed in cell culture medium, whereas we noted that the temperature of the medium had no significant effect on the rate of dissolution. The rate of dissolution of ZnO nanoparticles was somewhat higher in the presence of serum (Table 1). For comparison, the degree of dissolution of the SiO_2 nanoparticles was lower, and it was unaffected by the presence or absence of serum, whereas the TiO_2 and CeO_2 nanoparticles displayed very little, if any, dissolution. We also attempted to determine whether ZnO dissolution occurs in cells following coculture with the nanoparticles, using the cell-permeable, Zn^{2+}-sensitive fluorescent probe, Newport Green DCF. As seen in Supporting Information Figure 4B,C, Zn^{2+} ions were detected in cells after incubation with ZnO nanoparticles.

MGST1-Mediated Protection against Toxicity of Additional SiO_2 Nanoparticles. Finally, to assess whether the cytotoxicity of the SiO_2 nanoparticles studied herein is related to a particular batch of particles, we also tested four additional SiO_2 nanoparticles obtained from different commercial sources (see Materials and Methods). The size of the particles, ranging from 5 to 80 nm, was characterized by TEM (Supporting Information Figure 5A) as well as by DLS (Supporting Information Table 1). The particles were also characterized in terms of dissolution (in the presence or absence of serum) and zeta-potential (Supporting Information Table 1). Cytotoxicity was assessed using the MTT assay after exposure of cells for 24 h in cell culture medium without serum. As seen in Supporting Information Figure 6, three of the four SiO_2 nanoparticles exerted a pronounced dose-dependent cytotoxicity in the MCF-7 model. Overexpression of MGST1 protected against this cytotoxic effect in one of three cases. Thus, MGST1 protection against cytotoxicity triggered by amorphous SiO_2 nanoparticles is not a general phenomenon. In contrast to the main SiO_2 nanoparticles tested herein, the supplemental SiO_2 nanoparticles were more agglomerated (Supporting Information Table 1) and caused a very minor increase in mitochondrial ROS production (Supporting Information Figure 5B). The zeta-potential and rate of dissolution, however, were in the same range for the main SiO_2 nanoparticles and the four supplemental SiO_2 nanoparticles.

DISCUSSION

The cellular antioxidant enzyme, MGST1, is shown here to protect against SiO_2 nanoparticle-induced oxidative stress and cytotoxicity, while it failed to prevent ZnO nanoparticle-triggered cell death. Specifically, we find that overexpression of MGST1 protects against lipid peroxidation and oxidative damage triggered by SiO_2 nanoparticles. The results were confirmed using several different assays for cell viability/cell death, including short-term and long-term (colony formation) assays. However, the protective effect was not a general one for all amorphous SiO_2 nanoparticles

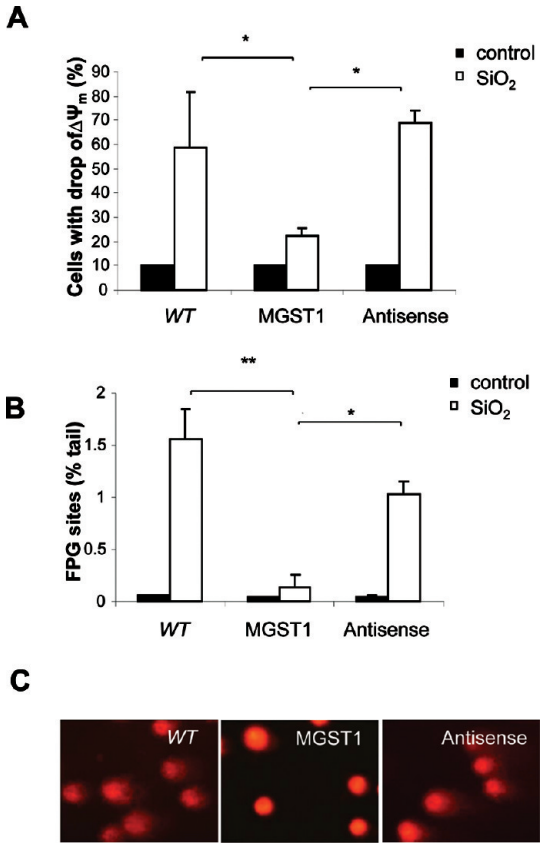

Figure 7. MGST1 protects against SiO_2 nanoparticle-induced mitochondrial depolarization (A) and oxidative DNA damage (B,C). Cells were incubated with 20 μg/mL SiO_2 nanoparticles for 2 h in the absence of serum. Fpg-comet assay was used to determine oxidative DNA damage (% of DNA content in the comet tail), and the TMRE assay was used for measurement of the dissipation of the mitochondrial transmembrane potential. Representative photographs depicting comet tails (seen in WT cells and antisense transfected cells) are shown. The data are expressed as mean values ± SD (n = 3); *<0.05, **<0.01.

since only a modest protection was observed for one out of three of the supplemental SiO_2 nanoparticles obtained from other sources. The possible reasons for the protection against some SiO_2 nanoparticles, but not against others, and for the lack of protection against the ZnO nanoparticles studied herein are discussed below. Previous studies have indicated that reactive silanol groups on the surface of silica particles may render such particles hemolytic.[23,24] On the basis of these observations, we may infer that the silanol groups on SiO_2 nanoparticles are involved in lipid peroxidation in critical cellular membranes, and that MGST1 protects cells from the formation of lipid hydroperoxides by reducing the hydroperoxides to lipid alcohol. This interpretation is supported by our recent work showing that MGST1 protects against lipid peroxidation triggered by cumene hydroperoxide and *tert*-butylhydroperoxide and by 4-hydroxy-2-nonenal, an end-product of lipid peroxidation.[14] On the other hand, MGST1 does not protect against cell death induced by ZnO nanoparticles, and we may therefore conclude that these nanoparticles trigger cell death through several mechanisms, not only through lipid peroxidation, including such pathways that are not effectively prevented by MGST1. In particular, ZnO nanoparticles may undergo dissolution, and Zn^{2+} ions may exert potent cytotoxic effects. Indeed, recent studies have disclosed that shedding of Zn^{2+} upon intracellular dissolution of ZnO nanoparticles induces lysosomal damage, elevation of intracellular calcium, mitochondrial perturbation, generation of ROS, and cell death.[4,25] In this context, it may be pertinent to note that we have utilized C_{11}-BODIPY$^{581/591}$ as a surrogate marker of lipid peroxidation. C_{11}-BODIPY$^{581/591}$ is a fluorescent fatty acid analogue that incorporates into cellular membranes in a heterogeneous manner, with no specific preference for any particular organelle, and with sparse staining of the plasma membrane.[26] Hence, although C_{11}-BODIPY$^{581/591}$ may be used as a probe to monitor lipid peroxidation, we cannot readily ascertain in which cellular compartment this lipid peroxidation is occurring, nor in which compartment or membrane(s) MGST1 is exerting its protective effect. At the highest concentration of SiO_2 nanoparticles, MGST1 showed no protection. This likely reflects the fact that the protective system is overwhelmed, but an alteration of toxic mechanism at high doses is also possible. Notwithstanding, our data point toward a central role for lipid peroxidation in SiO_2 nanoparticle-induced cytotoxicity. Based on the fact that overexpression of MGST1 prevents cell death, our data suggest, therefore, that oxidative stress plays a primary role in the cytotoxic actions of SiO_2 nanoparticles, whereas oxidative stress may instead be a secondary outcome of the ZnO-induced cellular insult. The fact that ZnO nanoparticles are capable of cell-free generation of ROS suggests that these particles may exert additional cytotoxic effects, not seen for SiO_2 nanoparticles. Moreover, one potential reason for the lack of protection against ZnO nanoparticle-induced cytotoxicity could be a direct inhibition of MGST1 by Zn^{2+} resulting from the dissolution of the particles and/or complexation of GSH by Zn^{2+}.

MGST1 is known to be highly expressed in rat liver, and recent studies have shown that MGST1 is overexpressed in certain tumors,[7] but its pattern of expression in normal human tissues has not been explored to date. We queried the publically available transcriptomics database, GENESAPIENS,[27] and noted high expression of MGST1 mRNA in the human liver and biliary system, as well as in mesothelium and adipose tissue (Supporting Information Figure 7). This suggests that the protective properties of MGST1 demonstrated in the present study may be highly relevant for tissues that come into contact with nanoparticles, for instance, upon entry of nanoparticles into the bloodstream. The subcellular localization of MGST1 in membranes,

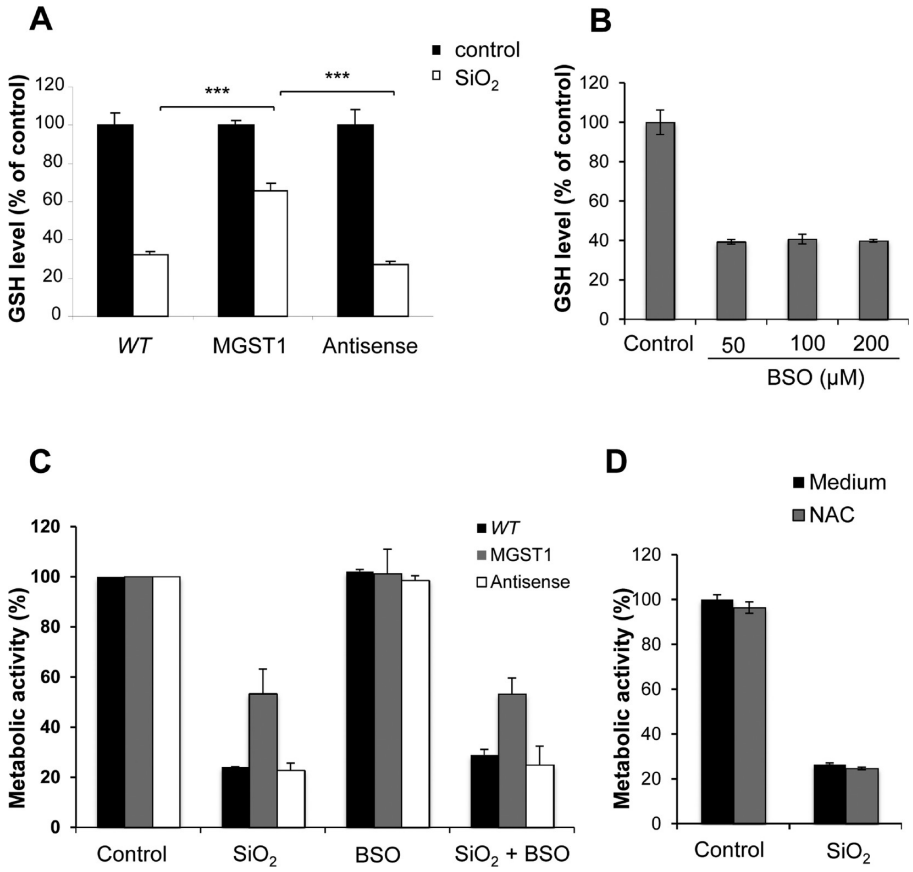

Figure 8. Intracellular glutathione (GSH) and toxicity of SiO_2 nanoparticles. ThioGlo-1 assay was used to determine GSH levels. (A) Exposure to SiO_2 nanoparticles (20 μg/mL, 2 h in the absence of serum) (A) results in a depletion of GSH, and this is reversed in MGST1 overexpressing cells. (B) Buthionine-[S,R]-sulfoximine (BSO)-induced depletion of intracellular GSH after 24 h. (C,D) Toxicity of SiO_2 nanoparticles (50 μg/mL, 24 h) is not affected by co-treatment with BSO (50 μM) (C) or *N*-acetylcysteine (NAC, 1 mM), a precursor of GSH.

particularly in mitochondrial and ER membranes,[8] further favors its role in protection against lipid peroxidation. Interestingly, recent gene expression profiling studies have demonstrated upregulation of MGST1 mRNA after exposure of cells to various types of engineered nanoparticles.[28,29]

An increased GSSG-to-GSH ratio is considered indicative of oxidative stress. MGST1 overexpression prevented the depletion of GSH induced by SiO_2 nanoparticles. However, neither the levels of GSH nor the activity of other major antioxidant enzymes such as cytosolic glutathione-S-transferase (GST), glutathione peroxidase (GPX), superoxide dismutase (SOD), or catalase, are altered in the cells that overexpress MGST1.[14] Moreover, we found that enforced depletion of GSH did not sensitize cells to SiO_2-induced toxicity, and addition of NAC, a precursor of GSH, failed to protect against SiO_2 nanoparticles. Furthermore, a recent study showed that lipid peroxidation induced by SiO_2 nanoparticles was independent of intracellular GSH levels.[30] Therefore, it seems likely that the protection from SiO_2-induced toxicity evidenced in the present study is due to a specific effect of MGST1, a microsomal enzyme that is distinct from cytosolic GSTs.[31] The subcellular localization of MGST1 (ER and outer membrane of mitochondria) points toward these organelles as critical sites of attack of cytotoxic SiO_2 nanoparticles.

Our TEM analyses clearly depicted SiO_2 nanoparticles interacting with the plasma membrane of MCF-7 cells, but it was difficult to establish their possible intracellular location due to the similarity in size and electron density to cellular structures such as ribosomes. However, FITC labeling of the SiO_2 nanoparticles and subsequent analysis using flow cytometry and fluorescence microscopy revealed cellular uptake of the particles both in the presence and in the absence of serum. These results, and the data demonstrating that the SiO_2 particles elicit mitochondrial ROS production, along with the reversal of this effect in cells that overexpress MGST1, are suggestive of a role for intracellular (mitochondrial) ROS for SiO_2 nanoparticle-induced cytotoxicity. Nevertheless, protection by MGST1 is also possible following particle interactions with the plasma membrane. Lipid peroxidation can generate reactive aldehydes such as 4-hydroxynonenal (HNE), which is rather long-lived when compared to free radicals, meaning that it can diffuse from the site of origin, for example, the cell membrane, and reach and

attack other intracellular targets. Indeed, we showed recently that MGST1 can protect MCF-7 cells against HNE toxicity.[14]

Oxidative stress has been associated with the cytotoxicity of various nanoparticles.[2] Nel and co-workers suggested that the cytotoxicity of different nanoparticles could be understood according to a so-called hierarchical oxidative stress paradigm.[2−4] For example, increased ROS production, elevated levels of lipid peroxidation, and a reduction in GSH content were observed in embryonic kidney HEK293 cells[32] and human bronchoalveolar carcinoma-derived A549 cells[33] upon exposure to amorphous silica nanoparticles. Induction of antioxidant enzymes, and involvement of oxidative stress-responding transcription factors such as NF-κB and Nrf-2, as well as the MAP kinase signal transduction pathway, was correlated with the cytotoxicity of fumed and porous silica nanoparticles in human bronchial epithelial cells.[34] Moreover, it has been shown that mesoporous silica nanoparticles impair mitochondrial respiration in various cell lines.[35] Our present findings are in accord with the latter observations, as we have observed that SiO_2 nanoparticles inhibit mitochondrial oxygen consumption in MCF-7 cells. Overexpression of MGST1 mitigated this effect to some degree. Similarly, we have recently provided evidence that mitochondria are strongly protected from the toxic effect of CuOOH by MGST1.[14] Pulmonary toxicity associated with oxidative stress was seen *in vivo* after intratracheal instillation of ultrafine colloidal silica particles.[36] ZnO nanoparticles were shown to induce increased levels of oxidative stress markers and to induce the expression of antioxidant genes such as heme oxygenase-1.[4,19,29,37,38] TiO_2 nanoparticles have also been shown to induce oxidative stress markers in different models.[39,40] CeO_2 nanoparticles were shown to induce oxidative stress in some models[41,42] and to act as ROS-scavenging agents in other studies.[4,43] Interestingly, alteration of the surface charge of CeO_2 nanoparticles was recently shown to change the cellular internalization, localization, and toxicity profile of these particles.[44] Surface functionality was also demonstrated to be important for the toxicity of silica−titania hollow nanoparticles.[45] We found that TiO_2 and CeO_2 nanoparticles are capable of inducing superoxide generation in MCF-7 cells (unpublished observations), yet these particles did not trigger cell death, thus further supporting the conclusion that ROS production *per se* is not equivalent to cytotoxicity but could also represent an adaptive response, as predicted by the hierarchical oxidative stress paradigm.[3]

Our results show that the lack of toxicity for the TiO_2 and CeO_2 nanoparticles was not due to a lack of cellular uptake. However, the lack of toxicity observed for the TiO_2 nanoparticles could perhaps be explained by the high extent of agglomeration in cell culture medium, as observed by DLS analysis. In addition, the supplementary SiO_2 nanoparticles displayed a greater degree of agglomeration when compared to the main SiO_2 nanoparticles in the present study and much less induction of mitochondrial ROS. This could explain why MGST1 overexpression failed to protect against the cytotoxicity of some of the latter particles.

ZnO nanoparticle toxicity was previously suggested to be due to leaching of Zn^{2+} ions both in cell culture medium and in endosomes.[4] In an elegant recent study, George *et al.* reported on the purposeful reduction of ZnO cytotoxicity by iron doping of the particles, which decreased the rate of nanoparticle dissolution.[25] Indeed, this strategy also yielded particles with reduced *in vivo* toxicity in rodent lung and zebrafish embryos.[46] Several studies have shown that Zn^{2+} ions inhibit cellular respiration.[47,48] It is also possible that Zn^{2+} may trigger extra-mitochondrial effects which are not prevented by microsomal enzymes such as MGST1. We find in the present study that ZnO nanoparticles leach Zn^{2+} ions in cell culture medium (12.3 and 17.7% dissolution in the absence and presence of serum, respectively), and Zn^{2+} ions were also detected within cells, and it is therefore likely that the cytotoxic effects of these nanoparticles are associated with particle dissolution. Moreover, our calculations indicated that the solubility of Zn^{2+} increases as the pH decreases (unpublished observations). This could explain the high degree of dissolution observed in H_2O (pH = 5−6) and suggests that these particles may undergo an even higher rate of dissolution in lysosomes following internalization by cells, as this is a highly acidic cellular compartment (pH = 4−5). The low recovery of free Zn^{2+} ions in PBS could be due to the higher pH (=7.4) but could also be explained by the formation of precipitates of Zn^{2+} ions and phosphate species. We noted that SiO_2 nanoparticles also undergo some dissolution when dispersed in cell culture medium (6.4 and 6.9% in the presence and absence of serum, respectively), but the silicic acid resulting from this dissolution is unlikely to contribute in a substantial way to cytotoxicity, as a recent study reported no cytotoxic or oxidative stress response of silicic acid arising from dissolution of porous silicon nanoparticles.[49] Furthermore, the supplemental SiO_2 nanoparticles showed a similar or higher rate of dissolution than the main SiO_2 particles in this study, albeit without showing higher toxicity toward MCF-7 cells, as evidenced by the MTT assay, again supporting the conclusion that silicic acid resulting from dissolution of the particles is not a main contributor to the toxic effects observed in this model.

Serum may impact cytotoxicity on several levels. First, serum withdrawal sensitizes cells to damage, and prolonged serum deprivation *in vitro* may trigger cell death. In addition, serum albumin, and other serum proteins, has been shown to serve as an antioxidant.[50] Hence, the protective effect of serum

against nanoparticle-induced cytotoxicity may be related to the antioxidant properties of serum proteins. Indeed, in our study, SiO_2 nanoparticle-induced cytotoxicity, as determined using the MTT assay, was reversed when the cell culture medium was supplemented with 10% FBS. However, the cytotoxic effects of SiO_2 nanoparticles in the presence of serum could be revealed in a long-term colony formation assay. Importantly, we show in this study that overexpression of MGST1 reduces SiO_2 nanoparticle-induced cytotoxicity in both short-term and long-term assays. On the other hand, we noted ZnO nanoparticle-induced cytotoxicity both in the presence and in the absence of serum, albeit slightly more so when serum was removed, likely due to Zn^{2+} ions binding to serum albumin. Similar results were obtained in a recent study of nanosized and submicrometer-sized SiO_2 particles.[51] In the presence of serum, no SiO_2 particles were toxic to HeLa cervical carcinoma cells. However, in the absence of serum, SiO_2 nanoparticles but not the larger SiO_2 particles were highly toxic. Drescher *et al.* reported similar effects of serum on SiO_2 nanoparticle toxicity in murine fibroblast 3T3 cells and suggested that this may be due to particle agglomeration in the presence of serum.[52] In addition, it has been shown that serum proteins bind to the surface of nanoparticles forming a so-called protein corona, which in turn may influence the biological/toxicological behavior of nanoparticles.[53,54] Monopoli *et al.* showed in a recent study that a protein corona is formed on SiO_2 nanoparticles even at low (3%) plasma concentration.[55] Interestingly, a "hard" protein corona was formed already after 1 h, and the thickness of the corona was reduced at higher plasma concentrations. These observations indicate that proteins may shield the silanol groups on the particle surface, resulting in less lipid peroxidation. Finally, serum proteins may also affect the cellular uptake of nanoparticles.[53,56] Indeed, higher cellular uptake was noted for the FITC-labeled SiO_2 nanoparticles in the absence of serum, which could potentially help to explain the higher toxicity evidenced under serum-free conditions. However, since the toxicity of the SiO_2 nanoparticles was completely inhibited in the presence of serum, the more likely explanation is that serum proteins shield reactive nanoparticle surfaces that otherwise would elicit cellular toxicity. It should be noted that the labeling of the SiO_2 nanoparticles by necessity changes the surface of the particles and the degree of agglomeration, and thus the actual uptake of the unmodified particles remains difficult to determine with certainty.

CONCLUSION

We show for the first time that the antioxidant enzyme MGST1 can protect cells against the cytotoxic effects of SiO_2 nanoparticles. These studies thus point to a prominent role for lipid peroxidation at the plasma membrane and/or at intracellular sites for SiO_2 nanoparticle-induced cytotoxicity. The hazardous effects of SiO_2 nanoparticles were reversed in the presence of serum, possibly due to the masking of reactive surface groups. The data presented here also indicate that the cytotoxicity of ZnO nanoparticles is triggered through a different pathway(s) likely related to the rapid dissolution of these particles in cell culture. These findings emphasize the existence of different mechanisms of cytotoxicity of different nanoparticles and point to protective strategies to overcome nanoparticle-induced adverse effects at the cellular level.

MATERIALS AND METHODS

Chemicals and Nanoparticles. Dulbecco's modified Eagle's medium (DMEM 41965) and supplements, including fetal bovine serum (FBS), sodium pyruvate, and penicillin-streptomycin, were obtained from GIBCO (Eugene, OR). Geneticin (G418) was purchased from GE Healthcare (Buckinghamshire, UK). The polyclonal rabbit IgG against rat MGST1 was generated in-house (R. Morgenstern). Horseradish peroxidase-labeled anti-rabbit IgG secondary antibody and primary antibody to β-actin were purchased from DAKO (Glostrup, Denmark). The Micro BCA protein reagent assay kit was from Pierce Biotechnology (Rockford, IL). Low melting point and normal melting point agarose were purchased from Fischer (Hampton, NH). ThioGlo-1 was purchased from Covalent Associates (Corvallis, OR). All other fluorescent probes were purchased from Molecular Probes (Leiden, The Netherlands). Cumene hydroperoxide (CuOOH), 3-[4,5-dimethylthiazol-2yl]-2,5-diphenyltetrazolium bromide (MTT), and zinc sulfate ($ZnSO_4$) were purchased from Sigma-Aldrich (St. Louis, MO). TiO_2 Aeroxide P25 was purchased from Degussa (Düsseldorf, Germany), CeO_2 cerium(IV) oxide 643009 was purchased from Sigma-Aldrich, ZnO zincoxTM 10 was purchased from IBU-tec (Weimar, Germany), and SiO_2 Ludox HS30 was purchased from DuPont (Wilmington, DE). The Cu nanoparticles used as a positive control in the acellular ROS assay were produced using the wire electroexplosive technique, as described previously.[57] Additional SiO_2 nanoparticles were purchased from Sigma-Aldrich, NanoAmor (Los Alamos, NM) and PlasmaChem (Mainz, Germany) (Supporting Information Table 1). Nanoparticles were dispersed in water and sonicated prior to cell culture experiments.

TEM, DLS, Zeta-Potential. Transmission electron microscopy (TEM) was performed on a LEO 912-Omega (Carl Zeiss, Jena, Germany) microscope, operating at 120 KV. Approximately 100 particles were counted per sample for size estimation, and the software ImageJ was used for data analysis. Dynamic light scattering (DLS) and zeta-potential measurements were done on a Zetasizer Nano ZS (Malvern Instruments, Malvern, UK) equipped with a 633 nm red laser. The DLS measuring solutions were prepared by dispersing the nanoparticles (10 μg/mL) in DMEM medium with or without 10% FBS, as indicated. DLS size estimates were based on the intensity and peak form according to standard procedures. For the zeta-potential measurement, the instrument uses laser Doppler electrophoresis to measure the net velocity of the nanoparticles in the liquid when an electric field is applied and then converts this to the zeta-potential.

ICP Analysis. For inductively coupled plasma (ICP) analysis, nanoparticles (1 mg/mL) were dispersed in H_2O (Milli-Q, Millipore, high purity water with a resistivity of 18 MΩ cm, pH = 5−6), PBS

(Medicago AB, analytical grade, pH = 7.4), or cell culture medium with/without serum. A motor with stirrer (Teflon) kept constant at a rate of 500 rpm was attached, and the temperature was kept constant by placing the flask tube in a glycerol oil bath and onto a thermal heater (Heidolph MR Hei-Standard, Schwabach, Germany). After 24 h, nanoparticles were separated from the aqueous solution using centrifugation (Hermle Labortechnik Z323, Wehingen, Germany) at 12 000 rpm for 15 min. Then the aqueous solution was further centrifuged at 80 000 rpm for 15 min at 10 °C using ultrahigh centrifugation (Optima TLX Ultracentrifuge 120 000 rpm Beckman Coulter, Brea, CA). The concentration of the relevant ions in the supernatant collected was determined using ICP-OES (iCAP 6000 Series Thermo Scientific, Waltham, MA). For each sample, 2−3 wavelengths were selected, and the axial plasma orientation was used for the analysis of ions in solutions. ICP standard solutions were used for the calibration curve, and the weight of the metal oxide nanoparticles was calculated from the obtained ICP analysis of the standards.

Cell Lines and Culture Conditions. The parental MCF-7 cell line (American Type Culture Collection, Manassas, VA) is a human breast carcinoma cell line with low endogenous expression of MGST1 and cytosolic GSTs. MCF-7 sense cells were transfected with a vector containing rat MGST1, and MCF-7 antisense cells were transfected with the antisense orientation of rat MGST1, as described previously.[9] Cells were maintained in Dulbecco's modified Eagle's medium (DMEM 41965) supplemented with sodium pyruvate and penicillin-streptomycin, with or without addition of 10% fetal bovine serum. Sense and antisense cells were maintained in the above medium supplemented with Geneticin (1 mg/mL G418).

Western Blot. Protein levels of MGST1 were determined as described previously.[9] Briefly, cells were lysed in 1% sodium dodecylsulfate (SDS) and 1% Triton X-100 in dH_2O. Twenty micrograms of protein was electrophoresed on a 15% SDS-polyacrylamide (SDS-PAGE) gel and transferred to a nitrocellulose membrane, which was probed with polyclonal rabbit IgG against rat MGST1 followed by horseradish peroxidase-labeled anti-rabbit IgG. Blots were developed using the enhanced chemiluminescence (ECL) kit (GE Healthcare). Membranes were reprobed with antibodies to β-actin to control for equal loading of protein.

LPS Analysis. Lipopolysaccharide (LPS) concentrations were controlled by the end-point chromogenic LAL test method (Limulus Amebocyte Lysate endochrome, Charles River Endosafe, Charleston, SC). The test results indicated endotoxin contamination levels of 1 ng/mL LPS in the Ludox HS30 SiO_2 nanoparticle sample but no detectable degree of endotoxin contamination for the other nanoparticles (Table 1). Repeated testing of three batches of SiO_2 nanoparticles from the same supplier revealed similar results. LPS concentrations of 1 ng/mL are sufficient to stimulate immune-competent cells.[58] However, in our pilot studies, LPS up to 1 μg/mL did not induce significant cell death in the MCF-7 cell line. Moreover, when MCF-7 cells were preincubated with the LPS-blocking agent polymyxin B (10 μM for 6 or 24 h) prior to addition of the nanoparticles, no changes were seen in cell viability or oxidative stress levels (unpublished observations). On the basis of these results, we concluded that endotoxin contamination was not responsible for the cytotoxic effects of nanoparticles reported in the present study.

Particle Uptake Using TEM. Cells were exposed to 50 μg/mL of the indicated nanoparticles in cell medium with/without fetal bovine serum for 2 h and were then washed with PBS, trypsinated, and centrifuged at 2000 rpm for 3 min. Cells were thereafter fixed in 2% glutaraldehyde in 0.1 M sodium cacodylate buffer containing 0.1 M sucrose and 3 mM $CaCl_2$, pH 7.4, and stored in refrigerator. Postfixation of pellets was carried out in 2% osmium tetroxide in 0.07 M sodium cacodylate buffer containing 1.5 mM $CaCl_2$, pH 7.4, at 4 °C for 2 h, dehydrated in ethanol followed by acetone, and embedded in LX-112 (Ladd, Burlington, VT). Sections were contrasted with uranyl acetate followed by lead citrate and examined in a Tecnai 12 transmission electron microscope (TEM) (Fei, The Netherlands) at 80 kV. Digital images were taken by a Veleta digital camera (Soft Imaging System, GmbH, Munster, Germany).

Cytotoxicity and Colony Formation Efficiency Assays. Short-term cell viability was determined by the 3-[4,5-dimethylthiazol-2yl]-2,5-diphenyltetrazolium bromide (MTT) assay, which reflects the mitochondrial function of cells.[59] Briefly, cells were seeded at a density of 1×10^4 cells/well in a 96-well plate, and after 24 h culturing, the medium was changed to DMEM without phenol red and serum. Four replicates were used for each concentration. After exposure, the supernatant was removed and cells were washed once with phosphate-buffered saline (PBS) (pH 7.4). One hundred microliters of MTT solution (0.5 mg/mL) was added and incubated for 3 h at 37 °C. Finally, 50 μL of dimethyl sulfoxide (DMSO) (Sigma Aldrich) was added to dissolve the formazan crystals. MTT conversion was quantified by measuring the absorbance at 570 nm using a spectrophotometer (Infinite F200, Tecan, Männedorf, Switzerland). In addition, short-term cell viability results were confirmed by the lactate dehydrogenase (LDH) assay (Roche Diagnostics, Indianapolis, IN). In brief, cells were plated in a 96-well plate at density of 1×10^4 cells/well. After exposure to nanoparticles for the indicated time points, 50 μL of supernatant was assayed for LDH activity following the manufacturer's protocol. The calculation of cytotoxicity percentage was as follows: Results are expressed as LDH content (%) = 100 − 100 × (exp LDH/max LDH) analyzed in triplicate from three or four independent experiments. Finally, the fluorescent dye propodium iodide (PI) was used to measure cell membrane permeability. To this end, cells were centrifuged, washed in PBS, and 50 μL/well PI (0.5 μg/mL) was added in a 96-well plate. Cells treated with Triton X-100 (0.2%) were used to determine maxiumum PI fluorescence, and cell death was expressed as percent of this value. Long-term effects on cell proliferation were ascertained using the colony formation efficiency (CFE) assay, as described previously.[9] Cells were seeded at a density of 50 cells/cm^2 in a 60 mm Petri dish. After 24 h, nanoparticles were added and cells were incubated for 24 h, and the cell culture medium was then replenished. After 7 days, cells were washed with PBS, fixed with 10% formalin, and stained with aqueous crystal violet, and colonies were counted manually under a light microscope. A colony was defined as consisting of at least 16 cells. Each experiment was repeated at least three times.

Flow Cytometric Assessment of ROS Production and Lipid Peroxidation. Fluorescent probes were incubated with cells at 37 °C in the dark prior to harvest as follows: (i) 5 μM MitoSOX for 10 min (assessment of mitochondria-generated superoxide), (ii) 25 nM TMRE for 20−30 min (assessment of mitochondrial membrane potential, $\Delta\psi_m$), (iii) 5 μM C11-BODIPY$^{581/591}$ for 30 min (a surrogate marker of lipid peroxidation).[18] Cells were trypsinized, neutralized with cell culture medium, and pelleted. For MitoSOX and C_{11}-BODIPY$^{581/591}$, cell pellet was resuspended with PBS; for TMRE, cell pellet was resuspended with HEPES buffer (10 mM HEPES-NaOH, 150 mM NaCl, 5 mM KCl, 1 mM $MgCl_2$, and 1.8 mM $CaCl_2$, pH 7.4). Flow cytometry was performed using a FACScan equipped with a 488 nm argon laser (Becton Dickinson) operating with CellQuestPro software (Becton Dickinson). MitoSOX and TMRE were analyzed in the FL-2 channel, while BODIPY$^{581/591}$ was analyzed in both FL-1 and FL-2. Cellular debris was gated out based on forward and side scatter characteristics. Ten thousand events were collected for each sample. For analysis of intracellular Zn^{2+}, the fluorescent probe Newport Green DCF was incubated with cells at a concentration of 5 μM for 30 min at room temperature in the dark. Cells were washed and incubated for a further 30 min at 37 °C. Cells were then fixed in 2% formaldehyde, permeabilized with 0.1% Triton X-100 in PBS, and analyzed by flow cytometry using a FACScan equipped with a 488 nm argon laser (Becton Dickinson) operating with CellQuestPro software (Becton Dickinson).

FITC Labeling of SiO_2 Nanoparticles. FITC labeling was performed similarly as previously described.[60] Briefly, the surface of the SiO_2 nanoparticles was first functionalized with amino propyl groups by reacting the particles with amino propyl triethoxy silane. The amine-functionalized particles were then reacted with FITC in ethanol under alkaline conditions in order to produce the imminothioester bond. Thermogravimetric analysis (TGA) confirmed the presence of tethered groups of propylamine and FITC within the sample at a loading level of

6 wt % (Supporting Information Figure 2). DLS measurements of these particles were performed as described above, and the data are reported in Supporting Information Figure 2.

Flow Cytometric Analysis of Particle Uptake. To study the internalization of FITC-labeled SiO_2 particles, MCF-7 cells were exposed to the FITC-labeled particles (20 μg/mL) in cell culture medium with/without serum for 2 h. Cells were washed with PBS and were then incubated with trypan blue (250 μg/mL) or PBS for 5 min. Cells were then washed again, trypsinated, centrifuged at 1600 rpm for 5 min, washed, and finally fixed with 2% formaldehyde. Flow cytometry was performed using a FACScan equipped with a 488 nm argon laser (Becton Dickinson) operating with CellQuestPro software (Becton Dickinson).

Fluorescence Microscopic Analysis of Particle Uptake. MCF-7 cells were exposed, and samples were prepared as described above for flow cytometric analysis. Following fixation, the cells were cytospun onto glass slides, and the cell nuclei were counterstained with DAPI (Sigma-Aldrich). Fluorescent images were acquired on a NIKON Eclipse TE-2000 fluorescence microscope equipped with a DS-5 M digital camera operating with NIS elements software (NIKON Instruments, Badhoeverdorp, The Netherlands).

FPG-Comet Assay. To investigate oxidative DNA lesions, the formamido-pyrimidine-glycosylase (fpg)-modified comet assay was applied as previously described[19] with the addition of the fpg enzyme (obtained from Prof. A. R. Collins, Department of Nutrition, School of Medicine, University of Oslo, Norway). Fifty cells were scored using fluorescence microscope (Leica DMLB, Houston, TX) with Comet Assay III software (Perceptive Instruments, Suffolk, UK), and a mean value of the DNA damage as percent tail of the comets was calculated for each sample. The level of fpg sites was obtained by subtracting the value of percent tail obtained with no enzyme added from the value when fpg enzyme was present.

GSH Assay. Intracellular reduced glutathione level was measured by an immediate fluorescence response upon the addition of ThioGlo-1 to cell homogenate, as previously described.[21] Fluorescence was measured using the Tecan Genios reader (Tecan Group Ltd., Männedorf, Switzerland) using excitation at 390 nm and emission at 485 nm. Protein concentration was measured with the Pierce BCA protein assay (ThermoScientific, Waltham, MA). In order to investigate whether alterations in intracellular GSH can modulate the toxicity of SiO_2 nanoparticles, MCF-7 WT cells were treated with 50, 100, and 200 μM buthionine-[S,R]-sulfoximine (BSO, Sigma-Aldrich) for 24 h, and the reduction in intracellular GSH was confirmed using the ThioGlo-1 assay. Furthermore, cells were coexposed to BSO (50 μM) and SiO_2 nanoparticles (50 μg/mL) for 24 h, and cytotoxicity was measured using the MTT assay. For some experiments, cells were also coexposed to SiO_2 nanoparticles (50 μg/mL) and *N*-acetylcysteine (NAC, Sigma-Aldrich) for 24 h, and cytotoxicity was evaluated using MTT assay, as described above.

Mitochondrial Function. Mitochondrial respiration was monitored as described previously.[61] In brief, MCF-7 cells were permeabilized with digitonin (5 μg/10^6 cells), and mitochondrial state 3 respiration (v3, actively respiring state) was stimulated by addition of succinate (5 mM), a substrate of Krebs cycle. State 4 (v4, nonphosphorylating) was attained after addition of oligomycin (3 μg/mL), an inhibitor of mitochondrial ATP synthase. The maximum activity of the respiratory chain was assessed upon addition of the protonophore, carbonyl cyanide *m*-fluorophenylhydrazone (FCCP) (1 μM). Measurement of respiration was performed at 30 °C. Changes in the oxygen concentration were monitored with an oxygen electrode (Hansatech Instruments, Norfolk, UK) and analyzed with the OxygraphPlus software (Hansatech Instruments).

ROS Production. To measure acelullar ROS production, a method similar to the one described by Rushton *et al.*[22] was used. In brief, sodium hydroxide (0.01 M) was added to 2′,7′-dichlorofluorescein diacetate (DCFH-DA) to cleave the DA from the DCFH. The reaction was stopped by the addition of sodium phosphate buffer (25 mM, pH 7.2), and immediately before use, horseradish peroxidase (2.2 U/mL) was added. This solution was incubated with the nanoparticles in final concentrations of 10, 40, and 100 μg/mL in 37 °C for 15 min. As positive controls, H_2O_2 (10 μM) and 10 μg/mL of Cu nanoparticles were used. The fluorescence was determined with excitation of 486 nm and emission 530 nm.

MGST1 Activity. MGST1 activity was tested by an assay that is based on the GST-catalyzed reaction between GSH and the GST substrate CDNB (1-chloro-2,4-dinitrobenzene), described elsewhere,[62] with the modification that Tris-HCl, pH was 7.0, was used instead of phosphate buffer (since Zn phosphate is insoluble).

Statistical Analysis. Data are expressed as mean values ± SD. Changes in variables were analyzed by paired Student's *t*-test or ANOVA with Tukey posthoc test. Differences between samples were considered to be significant at $P < 0.05$.

Conflict of Interest: The authors declare no competing financial interest.

Acknowledgment. This study was supported by the Seventh Framework Programme of the European Commission (FP7-NANOMMUNE, NMP-SL-2008-214281), Swedish Research Council, Swedish Council for Working Life and Social Research, Swedish Research Council for Environment, Agricultural Sciences and Spatial Planning and by the National Institutes of Health (to V.K.). J.S. is supported by a Ph.D. student grant from the Board of Postgraduate Studies at Karolinska Institutet (to B.F.). We thank Andrea Kunzmann and Carmen Vogt, Karolinska Institutet, for assistance with the endotoxin assay and TEM imaging of the supplementary silica nanoparticles, respectively. Dr. Kjell Hultenby, Electron Microscopy Core Facility, Karolinska Institutet, is acknowledged for expert assistance with electron microscopic determination of particle uptake.

Supporting Information Available: Figures S1−S7, described in the text, with accompanying figure legends, and supplementary Table 1. This material is available free of charge *via* the Internet at http://pubs.acs.org.

REFERENCES AND NOTES

1. Auffan, M.; Rose, J.; Bottero, J. Y.; Lowry, G. V.; Jolivet, J. P.; WiesnerM. R. Towards a Definition of Inorganic Nanoparticles from an Environmental, Health and Safety Perspective. *Nat. Nanotechnol.* **2009**, *4*, 634–641.
2. Xia, T.; Kovochich, M.; Brant, J.; Hotze, M.; Sempf, J.; Oberley, T.; Sioutas, C.; Yeh, J. I.; Wiesner, M. R.; Nel, A. E. Comparison of the Abilities of Ambient and Manufactured Nanoparticles To Induce Cellular Toxicity According to an Oxidative Stress Paradigm. *Nano Lett.* **2006**, *6*, 1794–1807.
3. Meng, H.; Xia, T.; George, S.; Nel, A. E. A Predictive Toxicological Paradigm for the Safety Assessment of Nanomaterials. *ACS Nano* **2009**, *3*, 1620–1627.
4. Xia, T.; Kovochich, M.; Liong, M.; Madler, L.; Gilbert, B.; Shi, H.; Yeh, J. I.; Zink, J. I.; Nel, A. E. Comparison of the Mechanism of Toxicity of Zinc Oxide and Cerium Oxide Nanoparticles Based on Dissolution and Oxidative Stress Properties. *ACS Nano* **2008**, *2*, 2121–2134.
5. Shvedova, A. A.; Kisin, E.; Murray, A. R.; Johnson, V. J.; Gorelik, O.; Arepalli, S.; Hubbs, A. F.; Mercer, R. R.; Keohavong, P.; Sussman, N.; *et al.* Inhalation *vs.* Aspiration of Single-Walled Carbon Nanotubes in C57BL/6 Mice: Inflammation, Fibrosis, Oxidative Stress, and Mutagenesis. *Am. J. Physiol. Lung Cell Mol. Physiol.* **2008**, *295*, 552–565.
6. Shvedova, A. A.; Kagan, V. E.; Fadeel, B. Close Encounters of the Small Kind: Adverse Effects of Man-Made Materials Interfacing with the Nano-Cosmos of Biological Systems. *Annu. Rev. Pharmacol. Toxicol.* **2010**, *50*, 63–88.
7. Morgenstern, R.; Zhang, J.; Johansson, K. Microsomal Glutathione Transferase 1: Mechanism and Functional Roles. *Drug Metab. Rev.* **2011**, *43*, 300–306.
8. Morgenstern, R.; Lundqvist, G.; Andersson, G.; Balk, L.; DePierre, J. W. The Distribution of Microsomal Glutathione Transferase among Different Organelles, Different Organs, and Different Organisms. *Biochem. Pharmacol.* **1984**, *33*, 3609–3614.
9. Johansson, K.; Ahlen, K.; Rinaldi, R.; Sahlander, K.; Siritantikorn, A.; Morgenstern, R. Microsomal Glutathione Transferase 1 in

Anticancer Drug Resistance. *Carcinogenesis* **2007**, *28*, 465–470.
10. Siritantikorn, A.; Johansson, K.; Ahlen, K.; Rinaldi, R.; Suthiphongchai, T.; Wilairat, P.; Morgenstern, R. Protection of Cells from Oxidative Stress by Microsomal Glutathione Transferase 1. *Biochem. Biophys. Res. Commun.* **2007**, *355*, 592–596.
11. Maeda, A.; Crabb, J. W.; Palczewski, K. Microsomal Glutathione S-Transferase 1 in the Retinal Pigment Epithelium: Protection Against Oxidative Stress and a Potential Role in Aging. *Biochemistry* **2005**, *44*, 480–489.
12. Mosialou, E.; Piemonte, F.; Andersson, C.; Vos, R. M.; van Bladeren, P. J.; Morgenstern, R. Microsomal Glutathione Transferase: Lipid-Derived Substrates and Lipid Dependence. *Arch. Biochem. Biophys.* **1995**, *320*, 210–216.
13. Mosialou, E.; Morgenstern, R. Activity of Rat Liver Microsomal Glutathione Transferase toward Products of Lipid Peroxidation and Studies of the Effect of Inhibitors on Glutathione-Dependent Protection Against Lipid Peroxidation. *Arch. Biochem. Biophys.* **1989**, *275*, 289–294.
14. Johansson, K.; Järvliden, J.; Gogvadze, V.; Morgenstern, R. Multiple Roles of Microsomal Glutathione Transferase 1 in Cellular Protection: A Mechanistic Study. *Free Radical Biol. Med.* **2010**, *49*, 1638–1645.
15. Kunzmann, A.; Andersson, B.; Thurnherr, T.; Krug, H.; Scheynius, A.; Fadeel, B. Toxicology of Engineered Nanomaterials: Focus on Biocompatibility, Biodistribution and Biodegradation. *Biochim. Biophys. Acta* **2011**, *1810*, 361–373.
16. Worle-Knirsch, J. M.; Pulskamp, K.; Krug, H. F. Oops They Did It Again! Carbon Nanotubes Hoax Scientists in Viability Assays. *Nano Lett.* **2006**, *6*, 1261–1268.
17. York, J. L.; Maddox, L. C.; Zimniak, P.; McHugh, T. E.; Grant, D. F. Reduction of MTT by Glutathione S-Transferase. *Biotechniques* **1998**, *25*, 622–624; 626–628.
18. Seiler, A.; Schneider, M.; Forster, H.; Roth, S.; Wirth, E. K.; Culmsee, C.; Plesnila, N.; Kremmer, E.; Radmark, O.; Wurst, W.; *et al.* Glutathione Peroxidase 4 Senses and Translates Oxidative Stress into 12/15-Lipoxygenase Dependent- and AIF-Mediated Cell Death. *Cell Metab.* **2008**, *8*, 237–248.
19. Karlsson, H. L.; Cronholm, P.; Gustafsson, J.; Moller, L. Copper Oxide Nanoparticles Are Highly Toxic: A Comparison between Metal Oxide Nanoparticles and Carbon Nanotubes. *Chem. Res. Toxicol.* **2008**, *21*, 1726–1732.
20. Karlsson, H. L. The Comet Assay in Nanotoxicology Research. *Anal. Bioanal. Chem.* **2010**, *398*, 651–666.
21. Kagan, V. E.; Kuzmenko, A. I.; Tyurina, Y. Y.; Shvedova, A. A.; Matsura, T.; Yalowich, J. C. Pro-oxidant and Antioxidant Mechanisms of Etoposide in HL-60 Cells: Role of Myeloperoxidase. *Cancer Res.* **2001**, *61*, 7777–7784.
22. Rushton, E. K.; Jiang, J.; Leonard, S. S.; Eberly, S.; Castranova, V.; Biswas, P.; Elder, A.; Han, X.; Gelein, R.; Finkelstein, J.; Oberdörster, G. Concept of Assessing Nanoparticle Hazards Considering Nanoparticle Dosimetric and Chemical/Biological Response Metrics. *J. Toxicol. Environ. Health A* **2010**, *73*, 445–461.
23. Slowing, I. I.; Wu, C. W.; Vivero-Escoto, J. L.; Lin, V. S. Mesoporous Silica Nanoparticles for Reducing Hemolytic Activity towards Mammalian Red Blood Cells. *Small* **2009**, *5*, 57–62.
24. Lin, Y. S.; Haynes, C. L. Impacts of Mesoporous Silica Nanoparticle Size, Pore Ordering, and Pore Integrity on Hemolytic Activity. *J. Am. Chem. Soc.* **2010**, *132*, 4834–4842.
25. George, S.; Pokhrel, S.; Xia, T.; Gilbert, B.; Ji, Z.; Schowalter, M.; Rosenauer, A.; Damoiseaux, R.; Bradley, K. A.; Madler, L.; Nel, A. E. Use of a Rapid Cytotoxicity Screening Approach To Engineer a Safer Zinc Oxide Nanoparticle through Iron Doping. *ACS Nano* **2010**, *4*, 15–29.
26. Drummen, G. P.; van Liebergen, L. C.; Op den Kamp, J. A.; Post, J. A. C11-BODIPY(581/591), an Oxidation-Sensitive Fluorescent Lipid Peroxidation Probe: (Micro)Spectroscopic Characterization and Validation of Methodology. *Free Radical Biol. Med.* **2002**, *33*, 473–490.
27. Kilpinen, S.; Autio, R.; Ojala, K.; Iljin, K.; Bucher, E.; Sara, H.; Pisto, T.; Saarela, M.; Skotheim, R. I.; Bjorkman, M.; *et al.* Systematic Bioinformatic Analysis of Expression Levels of 17,330 Human Genes Across 9,783 Samples from 175 Types of Healthy and Pathological Tissues. *Genome Biol.* **2008**, *9*, R139.
28. Huang, C. C.; Aronstam, R. S.; Chen, D. R.; Huang, Y. W. Oxidative Stress, Calcium Homeostasis, and Altered Gene Expression in Human Lung Epithelial Cells Exposed to ZnO Nanoparticles. *Toxicol. in Vitro* **2010**, *24*, 45–55.
29. Kedziorek, D. A.; Muja, N.; Walczak, P.; Ruiz-Cabello, J.; Gilad, A. A.; Jie, C. C.; Bulte, J. W. Gene Expression Profiling Reveals Early Cellular Responses to Intracellular Magnetic Labeling with Superparamagnetic Iron Oxide Nanoparticles. *Magn. Reson. Med.* **2010**, *63*, 1031–1043.
30. Akhtar, M. J.; Ahamed, M.; Kumar, S.; Siddiqui, H.; Patil, G.; Ashquin, M.; Ahmad, I. Nanotoxicity of Pure Silica Mediated through Oxidant Generation Rather than Glutathione Depletion in Human Lung Epithelial Cells. *Toxicology* **2010**, *276*, 95–102.
31. Morgenstern, R.; Guthenberg, C.; Depierre, J. W. Microsomal Glutathione S-Transferase. Purification, Initial Characterization and Demonstration That It Is Not Identical to the Cytosolic Glutathione S-Transferases A, B and C. *Eur. J. Biochem.* **1982**, *128*, 243–248.
32. Wang, F.; Gao, F.; Lan, M. B.; Yuan, H. H.; Huang, Y. P.; Liu, J. W. Oxidative Stress Contributes to Silica Nanoparticle-Induced Cytotoxicity in Human Embryonic Kidney Cells. *Toxicol. in Vitro* **2009**, *23*, 808–815.
33. Lin, W.; Huang, Y. W.; Zhou, X. D.; Ma, Y. *In Vitro* Toxicity of Silica Nanoparticles in Human Lung Cancer Cells. *Toxicol. Appl. Pharmacol.* **2006**, *217*, 252–259.
34. Eom, H. J.; Choi, J. Oxidative Stress of Silica Nanoparticles in Human Bronchial Epithelial Cell, Beas-2B. *Toxicol. in Vitro* **2009**, *23*, 1326–1332.
35. Tao, Z.; Morrow, M. P.; Asefa, T.; Sharma, K. K.; Duncan, C.; Anan, A.; Penefsky, H. S.; Goodisman, J.; Souid, A. K. Mesoporous Silica Nanoparticles Inhibit Cellular Respiration. *Nano Lett.* **2008**, *8*, 1517–1526.
36. Kaewamatawong, T.; Shimada, A.; Okajima, M.; Inoue, H.; Morita, T.; Inoue, K.; Takano, H. Acute and Subacute Pulmonary Toxicity of Low Dose of Ultrafine Colloidal Silica Particles in Mice after Intratracheal Instillation. *Toxicol. Pathol.* **2006**, *34*, 958–965.
37. Yang, H.; Liu, C.; Yang, D.; Zhang, H.; Xi, Z. Comparative Study of Cytotoxicity, Oxidative Stress and Genotoxicity Induced by Four Typical Nanomaterials: The Role of Particle Size, Shape and Composition. *J. Appl. Toxicol.* **2009**, *29*, 69–78.
38. Sharma, V.; Shukla, R. K.; Saxena, N.; Parmar, D.; Das, M.; Dhawan, A. DNA Damaging Potential of Zinc Oxide Nanoparticles in Human Epidermal Cells. *Toxicol. Lett.* **2009**, *185*, 211–218.
39. Liu, S.; Xu, L.; Zhang, T.; Ren, G.; Yang, Z. Oxidative Stress and Apoptosis Induced by Nanosized Titanium Dioxide in PC12 Cells. *Toxicology* **2010**, *267*, 172–177.
40. Park, E. J.; Choi, J.; Park, Y. K.; Park, K. Oxidative Stress Induced by Cerium Oxide Nanoparticles in Cultured BEAS-2B Cells. *Toxicology* **2008**, *245*, 90–100.
41. Eom, H. J.; Choi, J. Oxidative Stress of CeO_2 Nanoparticles *via* p38-Nrf-2 Signaling Pathway in Human Bronchial Epithelial Cell, Beas-2B. *Toxicol. Lett.* **2009**, *187*, 77–83.
42. Lin, W.; Huang, Y. W.; Zhou, X. D.; Ma, Y. Toxicity of Cerium Oxide Nanoparticles in Human Lung Cancer Cells. *Int. J. Toxicol.* **2006**, *25*, 451–457.
43. Tsai, Y. Y.; Oca-Cossio, J.; Agering, K.; Simpson, N. E.; Atkinson, M. A.; Wasserfall, C. H.; Constantinidis, I.; Sigmund, W. Novel Synthesis of Cerium Oxide Nanoparticles for Free Radical Scavenging. *Nanomedicine* **2007**, *2*, 325–332.
44. Asati, A.; Santra, S.; Kaittanis, C.; Perez, J. M. Surface-Charge-Dependent Cell Localization and Cytotoxicity of Cerium Oxide Nanoparticles. *ACS Nano* **2010**, *4*, 5321–5331.
45. Oh, W. K.; Kim, S.; Choi, M.; Kim, C.; Jeong, Y. S.; Cho, B. R.; Hahn, J. S.; Jang, J. Cellular Uptake, Cytotoxicity, and Innate Immune Response of Silica-Titania Hollow Nanoparticles

Based on Size and Surface Functionality. *ACS Nano* **2010**, *4*, 5301–5313.
46. Xia, T.; Zhao, Y.; Sager, T.; George, S.; Pokhrel, S.; Li, N.; Schoenfeld, D.; Meng, H.; Lin, S.; Wang, X.; *et al.* Decreased Dissolution of ZnO by Iron Doping Yields Nanoparticles with Reduced Toxicity in the Rodent Lung and Zebrafish Embryos. *ACS Nano* **2011**, *5*, 1223–1235.
47. Sensi, S. L.; Yin, H. Z.; Carriedo, S. G.; Rao, S. S.; Weiss, J. H. Preferential Zn^{2+} Influx through Ca^{2+}-Permeable AMPA/kainate Channels Triggers Prolonged Mitochondrial Superoxide Production. *Proc. Natl. Acad. Sci. U.S.A.* **1999**, *96*, 2414–2419.
48. Brown, A. M.; Kristal, B. S.; Effron, M. S.; Shestopalov, A. I.; Ullucci, P. A.; Sheu, K. F.; Blass, J. P.; Cooper, A. J. Zn^{2+} Inhibits Alpha-Ketoglutarate-Stimulated Mitochondrial Respiration and the Isolated Alpha-Ketoglutarate Dehydrogenase Complex. *J. Biol. Chem.* **2000**, *275*, 13441–13447.
49. Bimbo, L. M.; Sarparanta, M.; Santos, H. A.; Airaksinen, A. J.; Mäkilä, E.; Laaksonen, T.; Peltonen, L.; Lehto, V. P.; Hirvonen, J.; Salonen, J. Biocompatibility of Thermally Hydrocarbonized Porous Silicon Nanoparticles and Their Biodistribution in Rats. *ACS Nano* **2010**, *4*, 3023–3032.
50. Roche, M.; Rondeau, P.; Singh, N. R.; Tarnus, E.; Bourdon, E. The Antioxidant Properties of Serum Albumin. *FEBS Lett.* **2008**, *582*, 1783–1787.
51. Al-Rawi, M.; Diabaté, S.; Weiss, C. Uptake and Intracellular Localization of Submicron and Nano-Sized SiO(2) Particles in HeLa Cells. *Arch. Toxicol.* **2011**, *85*, 813–826.
52. Drescher, D.; Orts-Gil, G.; Laube, G.; Natte, K.; Veh, R. W.; Osterle, W.; Kneipp, J. Toxicity of Amorphous Silica Nanoparticles on Eukaryotic Cell Model Is Determined by Particle Agglomeration and Serum Protein Adsorption Effects. *Anal. Bioanal. Chem.* **2011**, *400*, 1367–1373.
53. Dutta, D.; Sundaram, S. K.; Teeguarden, J. G.; Riley, B. J.; Fifield, L. S.; Jacobs, J. M.; Addleman, S. R.; Kaysen, G. A.; Moudgil, B. M.; Weber, T. J. Adsorbed Proteins Influence the Biological Activity and Molecular Targeting of Nanomaterials. *Toxicol. Sci.* **2007**, *2100*, 303–315.
54. Ehrenberg, M. S.; Friedman, A. E.; Finkelstein, J. N.; Oberdörster, G.; McGrath, J. L. The Influence of Protein Adsorption on Nanoparticle Association with Cultured Endothelial Cells. *Biomaterials* **2009**, *30*, 603–610.
55. Monopoli, M. P.; Walczyk, D.; Campbell, A.; Elia, G.; Lynch, I.; Bombelli, F. B.; Dawson, K. A. Physical-Chemical Aspects of Protein Corona: Relevance to *In Vitro* and *In Vivo* Biological Impacts of Nanoparticles. *J. Am. Chem. Soc.* **2011**, *133*, 2525–2534.
56. Xing, X.; He, X.; Peng, J.; Wang, K.; Tan, W. Uptake of Silica-Coated Nanoparticles by HeLa Cells. *J. Nanosci. Nanotechnol.* **2005**, *5*, 1688–1693.
57. Midander, K.; Cronholm, P.; Karlsson, H. L.; Elihn, K.; Möller, L.; Leygraf, C.; Wallinder, I. O. Surface Characteristics, Copper Release, and Toxicity of Nano- and Micrometer-Sized Copper and Copper(II) Oxide Particles: A Cross-Disciplinary Study. *Small* **2009**, *5*, 389–399.
58. Vallhov, H.; Qin, J.; Johansson, S. M.; Ahlborg, N.; Muhammed, M. A.; Scheynius, A.; Gabrielsson, S. The Importance of an Endotoxin-Free Environment during the Production of Nanoparticles Used in Medical Applications. *Nano Lett.* **2006**, *6*, 1682–1686.
59. Kunzmann, A.; Andersson, B.; Vogt, C.; Feliu, N.; Ye, F.; Gabrielsson, S.; Toprak, M. S.; Buerki-Thurnherr, T.; Laurent, S.; Vahter, M.; *et al.* Efficient Internalization of Silica-Coated Iron Oxide Nanoparticles of Different Sizes by Primary Human Macrophages and Dendritic Cells. *Toxicol. Appl. Pharmacol.* **2011**, *253*, 81–93.
60. Witasp, E.; Kupferschmidt, N.; Bengtsson, L.; Hultenby, K.; Smedman, C.; Paulie, S.; Garcia-Bennett, A. E.; Fadeel, B. Efficient Internalization of Mesoporous Silica Particles of Different Sizes by Primary Human Macrophages without Impairment of Macrophage Clearance of Apoptotic or Antibody-Opsonized Target Cells. *Toxicol. Appl. Pharmacol.* **2009**, *239*, 306–319.
61. Schmidt-Mende, J.; Gogvadze, V.; Hellstrom-Lindberg, E.; Zhivotovsky, B. Early Mitochondrial Alterations in ATRA-Induced Cell Death. *Cell Death Differ.* **2006**, *13*, 119–128.
62. Morgenstern, R. Microsomal Glutathione Transferase 1. *Methods Enzymol.* **2005**, *401*, 136–146.